PCCP



View Article Online **PAPER**



Cite this: Phys. Chem. Chem. Phys., 2020, 22, 19903

Ultrafast spectroscopy of biliverdin dimethyl ester in solution: pathways of excited-state depopulation†

Yangyi Liu,^a Zhuang Chen,^a Xueli Wang,^a Simin Cao,^a Jianhua Xu, ^bab

Biliverdin is a bile pigment that has a very low fluorescence quantum yield in solution, but serves as a chromophore in far-red fluorescent proteins being developed for bio-imaging. In this work, excitedstate dynamics of biliverdin dimethyl ether (BVE) in solvents were investigated using femtosecond (fs) and picosecond (ps) time-resolved absorption and fluorescence spectroscopy. This study is the first fs timescale investigation of BVE in solvents, and therefore revealed numerous dynamics that were not resolved in previous, 200 ps time resolution measurements. Viscosity- and isotope-dependent experiments were performed to identify the contributions of isomerization and proton transfer to the excited-state dynamics. In aprotic solvents, a \sim 2 ps non-radiative decay accounts for 95% of the excited-state population loss. In addition, a minor ~30 ps emissive decay pathway is likely associated with an incomplete isomerization process around the C15-C16 double bond that results in a flip of the D-ring. In protic solvents, the dynamics are more complex due to hydrogen bond interactions between solute and solvent. In this case, the ~ 2 ps decay pathway is a minor channel (15%), whereas $\sim 70\%$ of the excited-state population decays through an 800 fs emissive pathway. The ~ 30 ps timescale associated with isomerization is also observed in protic solvents. The most significant difference in protic solvents is the presence of a >300 ps timescale in which BVE can decay through an emissive state, in parallel with excited-state proton transfer to the solvent. Interestingly, a small fraction of a luminous species, which we designate lumin-BVE (LBVE), is present in protic solvents.

Received 2nd June 2020. Accepted 11th August 2020

DOI: 10.1039/d0cp02971h

rsc li/pccp

Introduction

Bilins, such as biliverdin (BV) and its dimethyl ester (BVE) derivatives (Fig. 1, left) are spiral linear tetrapyrrole molecules that exhibit weak emission near 720 nm in solvents, with a quantum yield (QY) of $\sim 0.01\%$. When bound to proteins, the emission QY can be substantially higher. Far-red fluorescent proteins (FPs) based on bilin chromophores are being developed for bio-imaging with the aim of capitalizing on the deeper penetration of their longer-wavelength excitation and emission

[†] Electronic supplementary information (ESI) available: Data analysis methods; Fig. S1-S14 showing additional steady state and transient absorption results; Tables S1-S5 showing the corresponding fitting parameters for these data. See DOI: 10.1039/d0cp02971h

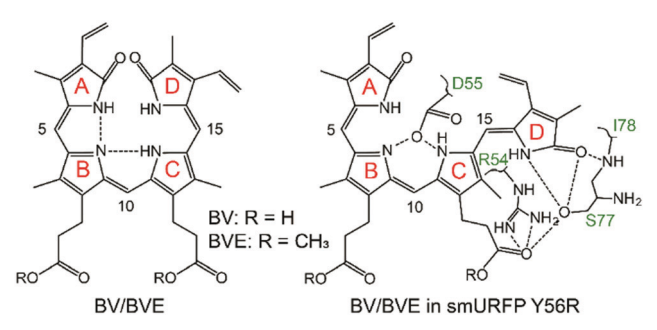


Fig. 1 The proposed intramolecular hydrogen bond structures of BV/BVE (left) and its binding site in smURFP Y56R (PDB: 6FZN, right).

through mammalian tissues.^{2,3} For example, smURFP was evolved from a subunit of allophycocyanin, a cyanobacterial light-harvesting biliprotein that covalently binds phycocyanobilin. smURFP was engineered to bind BV and achieve a relatively high fluorescence QY (18%).4 A crystal structure of smURFP is not yet available, except for that of a Y56R mutant, which has a low fluorescence QY (Fig. 1, right). Another family of far-red FPs was engineered from bacteriophytochromes (BphPs).

^a State Key Laboratory of Precision Spectroscopy, East China Normal University, Shanghai, China. E-mail: jqchen@lps.ecnu.edu.cn ^b Collaborative Innovation Center of Extreme Optics, Shanxi University, Taiyuan,

Shanxi 030006, China ^c National Institute of Standards and Technology and JILA, University of Colorado,

Boulder, CO, USA. E-mail: rjimenez@jila.colorado.edu

^d Department of Chemistry, University of Colorado, Boulder, CO, USA

In these signal transduction proteins, the covalently bound BV photoswitches between the red-absorbing (~700 nm) and far-red-absorbing (\sim 750 nm) ground state configurations.⁵⁻⁷ This photoconversion occurs via isomerization around the C15=C16 double bond and a subsequent proton transfer process across several amino acid side chains.^{8,9} FPs were generated by truncating the wild-type BphP, followed by several rounds of mutagenesis including structure-guided engineering of the BV binding site to inhibit the photoconversion and increase the fluorescence QY. The brightest FP of this family, miRFP670, has a fluorescence QY of 14%. A key to producing moderately emissive FPs in both cases, whether structural guidance is available or not, is to increase the excited-state lifetime by decreasing loss through non-radiative pathways such as proton transfer and photo-isomerization. A study of the excited-state dynamics of BVE in solution would provide important insights for further photophysical engineering of bilin-based FPs by revealing how the excited-state decays are influenced by solvent properties such as viscosity or polarity or by chromophore-solvent interactions such as hydrogen-bonding.

The most extensive photochemical investigations of BV, BVE, and several variants in solvents were reported by Braslavsky et al. who employed both steady-state and time-resolved spectroscopy with a 200 picosecond (ps) time resolution (full width at half maximum of the instrument response function). They proposed a model of BVE photo-isomerization coupled with excited state proton transfer based on C10=C11 bond torsion. 1,10,11 This mechanism contrasts with the more recent surface-enhanced Raman and infrared spectroscopy investigations as well as quantum chemistry calculations, which support the idea that isomerization at the C15=C16 bond is more probable than at C10=C11. 12-15 Recently, a nuclear magnetic resonance study showed that a small amount of deprotonated BV in solution forms a complex product with alcohols.16 Wang et al. synthesized three BV analogues and showed that isomerization can take place under the external influence of light and heat in different solution environments.6 Although the literature suggests that isomerization and proton transfer occur in bile pigments, many mechanistic details of isomerization and proton transfer in solvents were unresolved by the insufficient time resolution of the measurements.

We present the first femtosecond (fs) timescale experimental measurements on BVE in solution, including fluorescence up-conversion and transient absorption (TA), along with ps time-correlated single photon counting (TCSPC) results. The data reveal multiple solvent-dependent excited-state depopulation pathways of BVE. In aprotic solvents, BVE predominantly undergoes a non-radiative decay within a few picoseconds after excitation through a minor emissive decay pathway, which is associated with ring twisting and is reported here for the first time. In protic solvents, a sub-picosecond emissive decay channel appears and a BVE-to-solvent excited state proton transfer process occurs on a hundreds of picosecond timescale. A minor population of a new luminous species with a nanosecond (ns) excited-state lifetime was also observed in protic solvents. These results not only provide valuable information

for a comprehensive understanding of the excited state relaxation mechanism of BVE in solvents, but may also direct efforts for site-directed mutations to improve its fluorescence brightness in protein environments.

Experimental methods

Sample preparation

BVE (Frontier Scientific Inc.) was dissolved in solvents for spectroscopic experiments (30 µM). No vortex or ultrasound was used in order to avoid thermo-isomerization at room temperature (see details below and the ESI,† Fig. S1). All solvents (methanol, ethanol, *n*-propanol, deuterated methanol, acetonitrile, chloroform, acetone, and toluene) used in the experiment were purchased from Sigma-Aldrich. All mixed solution experiments mentioned in this work were performed by first mixing the solvents and then adding BVE. When ultrasonication was employed for specific experiments, a KS-80D ultrasonic oscillator (80 W, 40 kHz) was used.

Spectroscopy

A UV-Vis spectrophotometer (TU1901, Beijing Purkinje General Instrument Co. Ltd) and a FluoroMax-4 spectrofluorometer (Horiba, Jobin Yvon) were used to record steady-state absorption spectra and fluorescence spectra, respectively. The amount of LBVE increases continuously during the steady-state absorption, during fluorescence emission measurements or even without any treatment in the dark when it is in protic solvents. A fresh sample was used for each measurement.

TA spectra with a spectral range of 430 to 750 nm were acquired on a transient absorption spectrometer (Helios-EOS Fire, Ultrafast Systems) with a 1 kHz Ti:sapphire amplifier (Astrella, Coherent Inc.). Samples were held in a 2 mm fused silica cuvette. The instrument response function was determined to be ~ 120 fs by measuring solvent responses under the same experimental conditions.¹⁷ All measurements were performed at room temperature.

Femtosecond time-resolved fluorescence spectra were reconstructed from the single-wavelength fluorescence decay kinetics (670-740 nm) and were collected using a home-built fluorescence up-conversion setup which has been reported previously.¹⁸ In brief, the pump pulse is generated using an optical parametric amplifier (OPerA Solo, Coherent Inc.) and spectrally filtered by a pair of UV fused-silica prisms. The gate pulse is a small portion of an 800 nm fundamental beam. Fluorescence was collected using a pair of parabolic focus mirrors and then focused into a 0.5 mm Beta-BaB2O4 (BBO) crystal, which was used for sum frequency with the 800 nm gate pulse. Up-conversion signals were collected using a monochromator (Omnik500, Zolix) and detected using a photomultiplier tube (CR317, Hamamatsu). The time resolution was determined to be ~400 fs. Time-resolved emission spectra (TRES) were rebuilt from a global fitting of the fluorescence decay at different wavelengths using home-built MATLAB software. The specific procedure for data processing has been described in a previous study. 19

A home-built TCSPC system was used to measure fluorescence lifetimes.20 The excitation pulse was provided by a picosecond super-continuum fiber laser (SC400-pp-4, Fianium) with a repetition rate of 20 MHz, and fluorescence was recorded on a TCSPC module (PicoHarp 300, PicoQuant) and a microchannel plate-PMT (R3809U-50, Hamamatsu). A monochromator (7ISW151, Sofn Instruments) was used to select the emission wavelength. The time resolution of this equipment was 0.2 ns.

Results

Steady-state spectroscopy

The steady-state absorption and emission spectra of BVE in three different solvents are shown in Fig. 2a and b. The absorption band peak at \sim 660 nm is attributed to the $S_0 \rightarrow S_1$ transition. Additionally, a sharper absorption band with a peak at 375 nm was observed and it is assigned to the transition from the S₀ to an $S_{n>1}$ state.²¹⁻²³ The absorption spectra in CH₃CN and CHCl3 are nearly identical; however, BVE in methanol shows a 182 cm⁻¹ (from 658 nm to 666 nm) absorption redshift (Fig. 2a). The fluorescence emission spectra of BVE with 580 nm excitation (Fig. 2b) show a clear solvent dependence. In aprotic solvents

(CH₃CN and CHCl₃), as the polarity of the solvent increases, BVE emission shows a 397 cm⁻¹ redshift (from 700 nm in CHCl₃ to 720 nm in CH₃CN). On the other hand, the main emission peak is observed around 735 nm in CH₃OH while a new emission peak centered at 650 nm appears. It is unlikely that the new emission peak is due to the difference of solvent polarity. Also, the specific solvation effects, such as hydrogen bonding (H-bonding), preferential solvation, acid-base chemistry or charge-transfer interactions between solute and solvent, are a highly plausible explanation for this observation.²⁴ A concentration-dependence experiment was performed to exclude the effects of molecular aggregation. The absorption spectra are shown in Fig. S2a (ESI†) and no significant aggregate-characteristic absorption peak emerges with the increase of BVE concentration from 2 to 110 µM (Fig. S2a, ESI†). The area-normalized fluorescence emission spectra of the BVE-CH3OH solution treated with ultrasonication for varying durations is shown in Fig. S2b (ESI†). An isoemissive point could be clearly seen at ~705 nm, indicating that there are two emissive species in the BVE-CH₃OH solution. Moreover, the 650 nm emission peak was not observed for BVE in aprotic solvents where the molecule is most likely to be internally hydrogen-bonded (H-bonded), 25-27 and ring D could

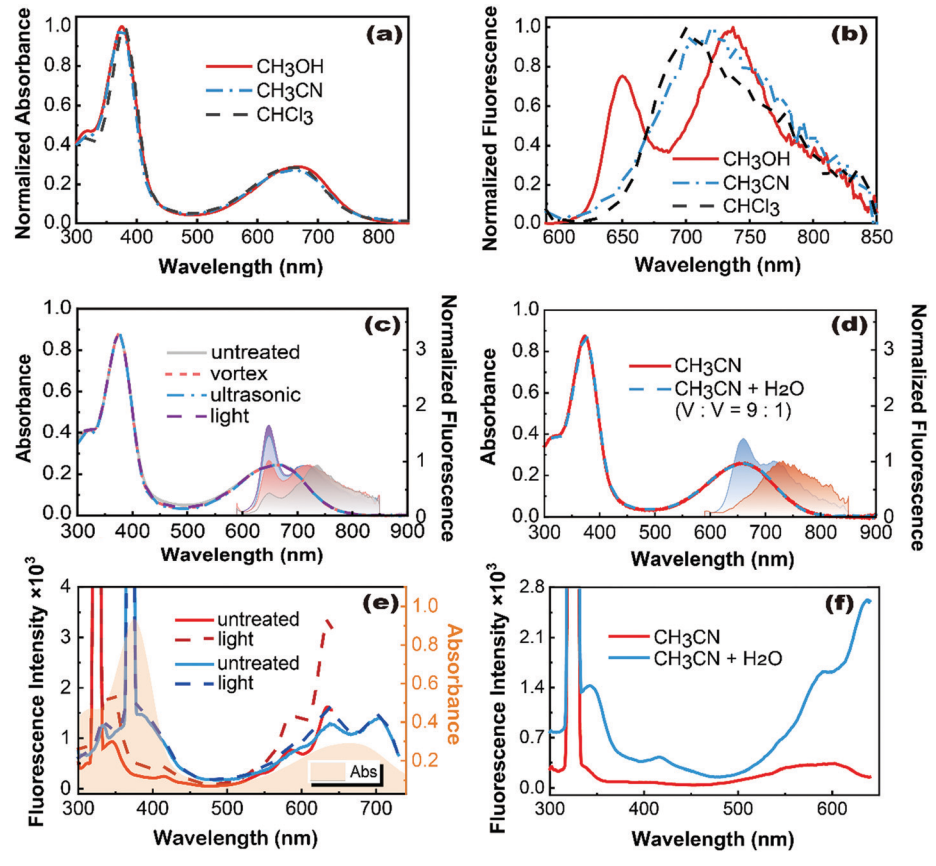


Fig. 2 Steady-state absorption (a) and fluorescence emission spectra (b) of untreated BVE. (c) Absorption (lines) and fluorescence emission spectra (color filled areas) of BVE in CH₃OH under different treatments (for 15 min). (d) Absorption and fluorescence emission spectra of BVE in CH₃CN (red) and a CH₃CN/H₂O mixture (blue dashes, keep it under fluorescence light for 15 min before measurements). (e) Fluorescence excitation spectra (lines) and absorption spectra (color filled areas) of BVE in CH₃OH under two detection wavelengths (red for 650 nm and blue for 740 nm). (f) Fluorescence excitation spectra (detected at 650 nm) of BVE in CH₃CN and a CH₃CN/H₂O mixture (under fluorescence light for 15 min).

Paper **PCCP**

retain a relatively stable dihedral angle toward the entire molecule via the π - π stacking effect, when the internal H-bond is intact (Fig. 1, left). Thus, it likely belongs to a new emission species with an extended, externally H-bonded form in the protic solvent, which we designate lumin-BVE (LBVE). The absorption and fluorescence spectra of BVE in other solvents are given in Fig. S3 (ESI†). While the absorption spectra of BVE show little change, the 650 nm emission peak appears again when the solvent is switched from aprotic (acetone and toluene) to protic (ethanol and *n*-propanol).

Braslavsky et al. reported the presence of a 650 nm emission peak for BVE dissolved in alcohols and ethyl acetate but ascribed it to a rigid stretched form of BVE, which would shielded by the aggregation effect in a high concentration solution.²⁸ However, our results support a different interpretation. First, we did not observe a concentration dependence of the absorption spectra over nearly the same range of concentrations. Second, the presence of an isoemissive point indicates that LBVE formation from BVE is described using a simple twostate model that is inconsistent with aggregation, in contrast to the previously recognized at least three species of BVE in the electronic ground state.

The influence of solvent and factors such as heat and light on formation of LBVE was examined. Fig. 2c exhibits the absorption and fluorescence emission spectra of BVE under four different treatments. Although the absorption spectra do not significantly change in shape, wavelength, or intensity, the increasing intensity of the 650 nm emission peak suggests that LBVE can be induced by either heat (vortex or ultrasonic) or light (laser irradiation or fluorescence light) in CH₃OH solution. No LBVE was observed in pure CH₃CN solution, but LBVE emission was observed in CH₃CN/H₂O mixtures (Fig. 2d).

The fluorescence excitation spectra of BVE in CH₃OH are shown in Fig. 2e. It is clear that the excitation spectra of BVE matched with the absorption spectra for the position of both high (380 nm) and low (700 nm) energy bands while more obvious vibronic peaks were seen at 590, 635 and 700 nm when the detection wavelength was 740 nm (blue line in Fig. 2e). There is only a small increase of the 635 nm peak after the sample is exposed to light (blue dashed line in Fig. 2e). The vibronic peaks at 590 nm and 635 nm reflect the contribution of LBVE, as the intensity varies after light irradiation. However, when the detection wavelength was set to 650 nm (red line in Fig. 2e), the excitation spectrum showed a change in shape relative to BVE (blue line in Fig. 2e). The low energy band shows a 1462 cm⁻¹ (from 700 nm to 635 nm) blue-shift and the high energy band shows a 2670 cm⁻¹ (from 380 nm to 345 nm) shift. Moreover, a small but distinct new peak appears near 420 nm. The intensity of the whole spectrum increases after sample is exposed to light, indicating that the main contributor of fluorescence at 650 nm is LBVE. Furthermore, the excitation spectra (Fig. 2f) clearly show the appearance of LBVE when H₂O is added to CH₃CN after the solution is exposed to light. A violation of the Kasha rule is evident from the fluorescence excitation spectra of BVE when excited in the high-energy band at 375 nm, which suggests that there are other decay channels

than the S_2 to S_1 internal conversion in the higher excited states. Actually, photo-induced Z-E isomerization has been reported in bilirubin (which has very similar structure to BVE) when higher excited states were populated by two-photon excitation.²⁹

Picosecond fluorescence dynamics of BVE in CH₃OH

TCSPC experiments were carried out on untreated and ultrasonically treated BVE-methanol solutions in order to show the dramatic difference in the fluorescence lifetimes of BVE and LBVE. Fluorescence decay kinetics are given in Fig. 3 and corresponding fitting data are listed in Table S1 (ESI†). Four fluorescence lifetimes were determined. The fastest, instrumentlimited decay has the highest amplitude, indicating that the major excited state deactivation in CH3OH takes place faster than the 0.2 ns time resolution of the TCSPC instrument. The second lifetime, τ_2 , was found to be ~ 0.5 ns and we discuss its origin in detail below. Experiments in which the detection wavelength is close to the 650 nm emission band of LBVE lead to unique values for τ_3 and τ_4 . The lifetimes were determined to be \sim 1 ns and 4.5 ns, respectively. The amplitudes of both τ_3 and τ_4 increased in the BVE solution after ultrasonic treatment. Although τ_3 and τ_4 both own a small proportion of the total amplitude, the fluorescence intensity of LBVE is comparable to that of the main emission peak (Fig. 2b and c). LBVE therefore has approximately an order of magnitude higher fluorescence QY than BVE, as expected from the observed much longer excited state lifetime (see details below).

Fluorescence up-conversion spectroscopy

Femtosecond time-resolved fluorescence up-conversion kinetics of BVE in CH₃OH are displayed in Fig. 4a. Decayassociated spectra (DAS) were extracted from the global fitting of these kinetics and the TRES was also reconstructed (Fig. 4b and c). Fig. 4d depicts the intensity-normalized TRES and it shows that the maximum emission peak shifts continuously in the first 8 ps after excitation. Femtosecond time-resolved fluorescence up-conversion measurements were also carried out in CHCl3 solutions. The representative kinetics at 720 nm are shown in Fig. S5 (ESI†) to compare with that in CH₃OH. It is clear that the ultrafast and the hundreds of picosecond components were missing for BVE in CHCl₃.

Femtosecond transient absorption spectroscopy

The results of TA measurements are shown in Fig. 5. In both CHCl₃ and CH₃OH solutions, there are two contributions to the TA signals. The first one is an excited state absorption (ESA) band ranging from 430 to 600 nm and the other is a ground state bleach (GSB) centered around 660 nm. No obvious stimulated emission signal was found in the TA data, possibly due to the spectral overlap with the more intense GSB and ESA signals. In CHCl₃, no shift was observed in the ESA or the GSB signal, and both signals decay to the baseline of ~ 10 ps after excitation. The TA spectra of BVE in CH₃OH are quite different. First of all, there is an obvious \sim 730 cm⁻¹ redshift (Fig. S6, ESI†) of the ESA band from 0.2 ps to 2 ps while the GSB signal remains at 660 nm. Secondly, the excited state lifetime is much longer in

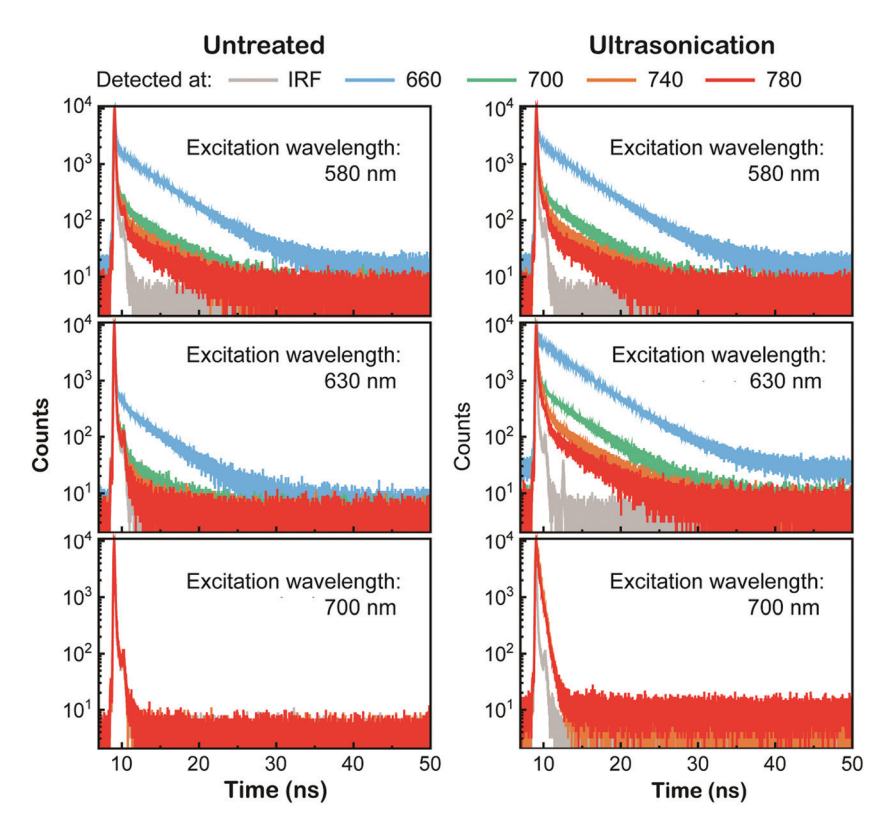


Fig. 3 Time-resolved fluorescence decays of BVE in CH₃OH

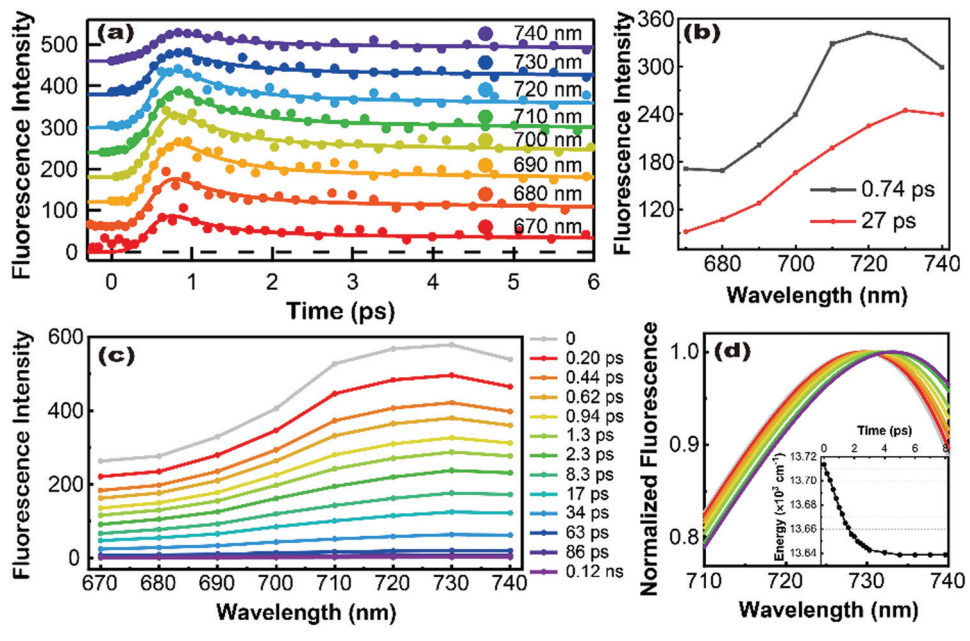


Fig. 4 (a) Fluorescence up-conversion data for of BVE in CHCl₃ (630 nm excitation). Lines represent the best fitting results. DAS (b) and TRES (c) are given in order. Illustration in intensity-normalized TRES (d) in the time range of 0-8 ps. The inset in panel (d) is given to show that the energy of the maximum emission peak decreased non-linearly versus time.

CH₃OH, and the TA spectra take several hundreds of picoseconds to return to the baseline.

Global analysis was performed on the TA spectra of BVE in solvents, and the spectral evolution was visualized by determining both the decay-associated spectra (Fig. S7, ESI†) and the evolutionassociated difference spectra (EADS). The single-wavelength kinetics at the representative wavelengths are shown in Fig. S8 (ESI†). In CHCl₃, two components were required with lifetimes



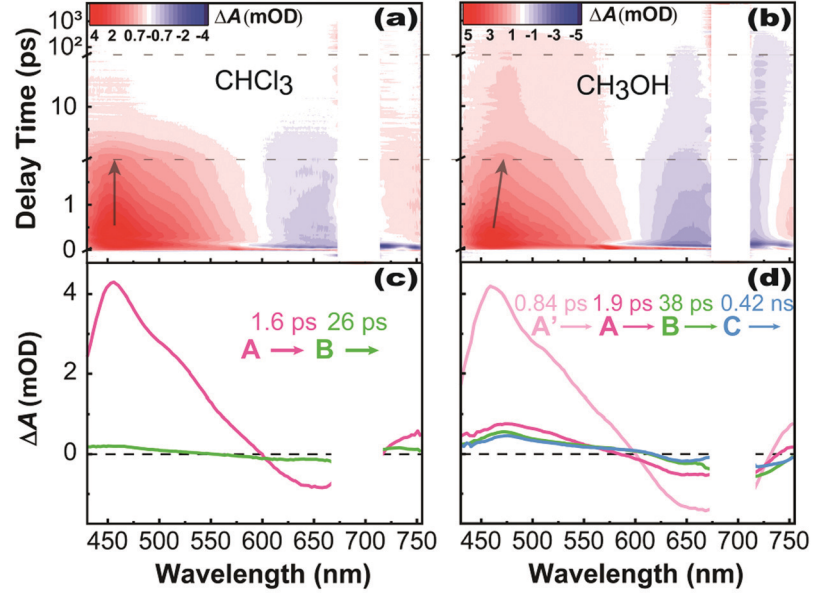


Fig. 5 Broadband transient absorption spectra of BVE in (a) CHCl₃ and (b) CH₃OH. (c and d) Represent the corresponding evolution-associated difference spectra (EADS) from global fitting.

of 1.6 ps and \sim 25 ps (Table S3, ESI†). The corresponding EADS are shown in Fig. 5c. The first EADS (red) at 1.6 ps shows an ESA band at around 430 nm and a GSB band at around 660 nm. It converts into the second EADS (green) and decays back to the baseline with a lifetime of ~ 25 ps. Since the EADS of the 1.6 ps component shows an obvious loss of GSB amplitude during evolution, it most likely represents the major excited state depopulation channel. On the other hand, the ~ 25 ps component, which closely corresponds to time constants in the up-conversion experiment, is the emissive deactivation channel.

In CH₃OH, four time constants were determined. The first EADS (pink) with an 840 fs lifetime has an ESA band at around 460 nm and a GSB band at around 660 nm. It turns into the second EADS (red) with a redshift of the ESA band to 470 nm as well as an obvious loss of ESA and GSB signal amplitudes. The second EADS changes into the third one (green) with a lifetime of 1.9 ps. There is a further ~5 nm redshift of the ESA band along with a slight loss of ESA and GSB amplitudes. The third EADS (green) decays with a lifetime of 38 ps and the fourth EADS (cyan) shows an excited state decay with a lifetime of 420 ps.

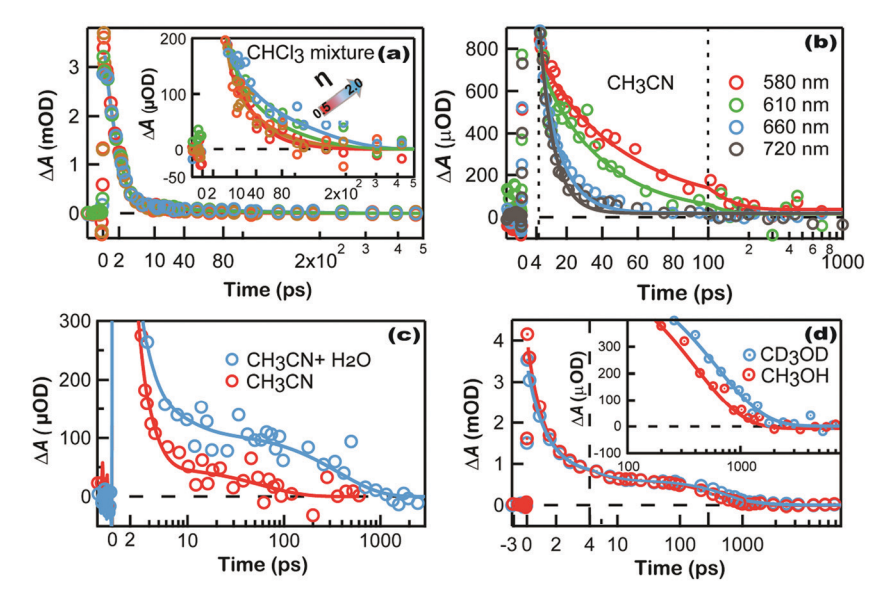


Fig. 6 Kinetics of BVE (pumped at 700 nm and probed at 460 nm) in (a) a CHCl₃ mixture (inset shows increasing lifetime vs. viscosity). (b) BVE in CH₃CN at the indicated pump wavelength (data are shown logarithmically after 100 ps). (c) BVE in CH3CN and a CH3CN/H2O mixture (data are shown logarithmically after 2 ps). (d) BVE in CH₃OH and CD₃OD (data are shown logarithmically after 4 ps and the inset shows the difference at longer time delays).

Viscosity-dependent TA experiments were conducted on BVE solutions. By adding tetraethylene glycol dimethyl ether into CHCl₃, the viscosity was tuned from $0.532\eta/(mPa~s)$ to $2.040\eta/(mPa~s)$. The kinetics at 490 nm are displayed in Fig. 6a and the global fitting results are listed in Table S5 (ESI \dagger). The value of τ_2 increases from 25 ps to 102 ps with η while τ_1 remains unchanged.

As early as the 1980s, Velsko and Fleming have shown that solution temperature and viscosity are closely related to molecular photochemical isomerism (in which the twisting process must occur).³⁰ And, the viscosity (η) dependence of the relaxation lifetime (τ) for various cyanine dyes in different solvents is reported to be close to either $\eta^{\frac{2}{3}}$ or η^1 . The case of $\tau = C\eta^{\frac{2}{3}}$ was reported by Taylor et al.³¹ and was seen as a confirmation of the validity of the Forster and Hoffman (FH) theory. In 1981, Sundstrom et al. explored the relationship between the viscosity of radiationless relaxation and concluded that the relationship between τ and η can be described by eqn (1) if it is related to the torsion motion.³²

$$\frac{1}{\tau} = C\eta^{-\alpha} \tag{1}$$

Here C is a constant and depends on different situations and α is a parameter which can be used to characterize the viscosity dependence of the radiationless relaxation rate. A similar method was applied to BVE, and the plot of $\log \tau$ versus $\log \eta$ (Fig. S9, ESI†) was fitted with a straight line with an R^2 value of 0.99 and a slope of 1.04 \pm 0.04.

Wavelength-dependent TA experiments at four different excitation wavelengths were performed on BVE in CH3CN (Fig. S10, ESI†). The kinetics at 460 nm are shown in Fig. 6b. The amplitude of the \sim 25 ps component at 460 nm decreases from 20% to less than 1% as the excitation wavelength is tuned to the low frequency region.

To verify the origin of the longer-lived (> 300 ps) component, water was added to CH₃CN (v:v = 1:9) to introduce H-bond acceptors into the solvent mixture, which compete with the intramolecular H-bond in BVE after photo-excitation. Fig. 6c shows the kinetics for BVE in CH₃CN and a CH₃CN/ H₂O mixture. Full TA data and the corresponding EADS are given in Fig. S11 (ESI†). Fitting results are listed in Table S3 (ESI†). Compared with BVE in CH₃CN, a fast decay component with τ_1 = 0.81 \pm 0.1 ps and a new longer-lived component (350 \pm 30 ps) were observed in CH₃CN/H₂O mixtures. TCSPC measurements also confirmed the luminescence properties of this longer-lived component (Fig. S12 and Table S1, ESI†). Four lifetime components were observed in CH₃CN/H₂O mixtures. The time constant τ_1 , which is smaller than the instrument response function (0.2 ns), accounts for the highest amplitude. Time constants τ_2 and τ_3 were observed only when the detection wavelength was close to the main fluorescence emission peak (~725 nm for BVE in the CH₃CN/H₂O mixture) and the newly emerged fluorescence emission peak at 650 nm, respectively. The time constant τ_4 is an ns timescale component similar to the one observed in LBVE. A series of lifetimes very close to those in BVE CH₃OH solution were observed when a

small percentage of water was added to the BVE CH3CN solution, indicating that similar excited state relaxation pathways appeared, which are directly regulated by the H-bonding environment of BVE, although BVE has no significant interaction with water molecules in the ground state.

Discussion

BV is often described as a linear tetrapyrrole molecule; however, the conformation is more typically helical, whether in solution or on a metal surface. 27,33,34 The double bonds between the B and C rings of BVE give rise to a flatter molecular structure and produce a more delocalized π -electronic cloud than bilirubin, which has a main absorption peak at \sim 450 nm. Bilirubin has a tetrahedral carbon in the methylene bridge, which allows for the free rotation of each half of the molecule.³⁴ At the same time, intramolecular H-bonds also play an important role in the conformational stability of these two bile pigments. Bilirubin relies on H-bond interactions between the carboxylic acid side chain and the imino on the pyrrole ring to form a stable "ridge tile" comformation whereas BVE utilizes the unsaturated nitrogen on the pyrrole ring to form internal H-bonds between the amino groups so as to increase overall molecular planarity. 35 When these H-bonds change, the configuration of bilirubin and the way it dissipates excited-state energy are greatly affected accordingly. 29,36,37 Therefore, it is reasonable to expect that the excited-state dynamics of BVE are related to its molecular configuration, which can be altered by the external environment.

Solvent dependence of the excited-state dynamics of BVE

As shown above, the excited-state dynamics of BVE in aprotic solvents such as chloroform and anhydrous acetonitrile are much simpler than in a protic environment. The absence of new emission peaks (Fig. 2b and Fig. S3, ESI†) or the spectral shift of the ESA band in TA spectra (Fig. 5a and Fig. S11a, ESI†) suggests that intramolecular H-bond changes do not occur. For BVE in CHCl₃, a major loss of the GSB signal (>95% amplitude) takes place on a 1.6 ps timescale (Fig. 5c and Table S3, ESI†). The mirror-image ESA and GSB decay kinetics (Fig. S8, ESI†) indicate that depopulation of the excited state leads to a direct repopulation of the ground state. This process is a "dark" channel since it is not observed in the fluorescence up-conversion experiment. Due to the low fluorescence QY $(<0.01\%)^{38}$ and intersystem crossing yield $(<0.004)^{39}$ of BVE, internal conversion has to be the dominant excited-state deactivation channel. Internal conversion through conical intersections (CIs) is an effective pathway of excited-state population loss in many biomolecules such as DNA nucleobases40 and p-hydroxybenzylidene-2,3-dimethylimidazolinone in GFP. 41-44 Previous studies have proposed ultrafast internal conversion through CIs in bilirubin in solvents and in a protein environment.37,45 Furthermore, ring deformation and N-H stretching have also been shown to lead to CIs between the excited and ground states in one single pyrrole ring. 46-48 Thus, it **Paper**

is not surprising that decay through CIs could occur in BVE since it has a high structural similarity to bilirubin.

Although its amplitude is less than 5% in the TA spectra, the second EADS component of BVE in CHCl₃ is the main luminous state, which was confirmed by the fluorescence up-conversion experiment (32 ps, 83% amplitude). A similar lifetime was reported for bacteriophytochromes and it was attributed to the twisting of ring D in the excited state.8 However, there was no direct evidence of molecular twisting in the previous study. In this work, we have shown that the lifetime of the second EADS component (τ_2) is affected by solvent viscosity (Fig. S9, ESI†). Good linearity between $\log \tau_2$ and $\log \eta$ indicates that molecular torsion dominates the non-radiative transition and that other non-radiative transition processes are negligible. 31,49,50 Therefore, τ_2 (~30 ps lifetime in CHCl₃) is a decay process directly associated with BVE molecular twisting in the excited state even though it is a minor decay channel (<5%). It is difficult to determine the specific site of the twisting in BVE using only our current TA data. As mentioned above, it has been reported that the C15=C16 bond in BVE is the most likely twisting site in the protein environment.¹⁵ Molecular dynamics simulations and quantum/ molecular mechanics calculations also suggest that Pr/Pfr photoswitching of BV-based FPs is most likely associated with a change in the protonation state on the D ring.⁵¹ Similarly, we suggest that the excited-state timescale associated with torsional dynamics reflects energy dissipation through torsion of the D ring.

The excited-state dynamics of BVE in protic solvents is more complex. A faster decay component, with a 0.84 ps lifetime (58%) appears and it corresponds to the loss of the majority of the GSB signal (Fig. 5). It also corresponds to the 0.74 ps time constant in our fluorescence up-conversion results (Fig. 4), suggesting that this is a bright excited-state deactivation channel, which does not exist in aprotic solvents. The second EADS, with a 1.9 ps lifetime, can be assigned to the same decay channel found in CHCl₃, which leads to a loss of the GSB signal but does not appear in the up-conversion data. Moreover, while the 38 ps component is still present, an additional ~ 0.4 ns time constant was determined in both TA and up-conversion experiments. It has been reported that protonation states of BV and its analogs can change and they can form a complex with solvent molecules when they are in alcohols. 16 Thus, we propose that the disturbance of intramolecular H-bonds and the H-bond interaction between the solvent and BVE are the key reasons for the appearance of the 0.84 ps and \sim 0.4 ns excitedstate relaxation pathways. For the 0.84 ps component, it should be assigned to a new ultrafast decay pathway induced by the perturbation of the BVE intramolecular H-bonds as well as the ultrafast solvation process of BVE in CH₃OH. It is reasonable that there are more vibrational modes enabled due to the loss of intramolecular H-bonds in BVE. Therefore, intramolecular vibrational energy redistribution from Franck-Condon active modes to fluorescence emissive modes could occur readily and lead to this ultrafast, bright decay channel.⁵² For the ~ 0.4 ns decay component, an isosbestic point appeared at 585 nm in the EADS (Fig. S6, ESI†) and the ESA signal increased (570-620 nm) as the third EADS (green) evolved to the fourth

EADS (cyan). This result suggests that the 38 ps component is an intermediate state to the longer-lived state. We have also conducted TA experiments on BVE in deuterated CH₃OH (Fig. 6d) and found that only the 0.4 ns component was affected. The kinetic isotope effect value was determined to be 1.6 (Table S3, ESI†), indicating that this component is related to excited state proton transfer, as discussed below.

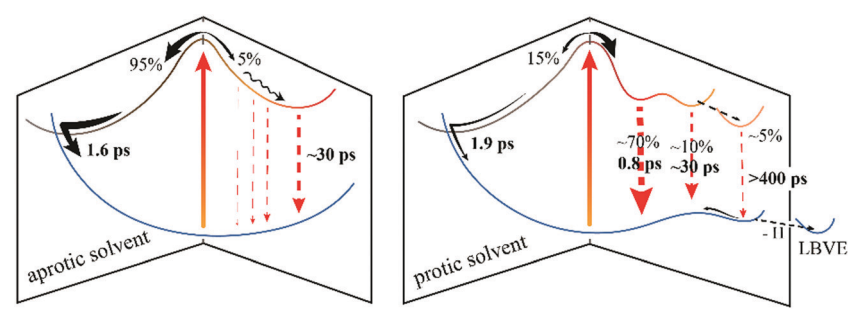
The emissive species LBVE

With the addition of a protic solvent, a new emission peak appears in the steady state fluorescence spectra. As shown in Fig. 2b-d, the intensity of the 650 nm emission component increases with vortexing, ultrasound and light illumination, while the absorption remains almost unchanged. Area normalized fluorescence emission spectra (Fig. S2b, ESI†) demonstrate the two-state conversion of BVE to LBVE, which has a 1462 cm⁻¹ nm blueshifted absorption spectrum (Fig. 2e). The Stokes shift of BVE is 579 cm $^{-1}$, while it is 363 cm $^{-1}$ for LBVE, which is consistent with a more rigid structure for the latter. The fluorescence decay timescales of LBVE (1.2 and 4.6 ns) are much longer and are consistent with its 37-fold higher fluorescence QY, which is estimated in the ESI† by considering the amount of BVE converted to LBVE and the resulting increase of the fluorescence intensity (Fig. S13, ESI†). Interestingly, the 0.37% fluorescence QY of LBVE in CH₃OH is still 3-fold smaller than the 1% fluorescence QY of smURFP Y56R, although its Stokes shift is smaller (468 cm⁻¹ in the latter). Taking into account that the Stokes shift is 650 cm⁻¹ in smURFP, which has an 18% OY, it appears that a smaller Stokes shift does not correlate with a higher fluorescence yield in this chromophore. This trend is the opposite of the more common observation that a smaller Stokes shift is a metric for rigidity, which in turn is correlated with the higher fluorescence QY of many chromophores.⁵³ However, the Stokes shift may be insufficient for characterizing the rigidity of tetrapyrrole chromophores due to the structural heterogeneity associated with their highly flexible structure and the presence of multiple forms (see below). In addition to structral information, a level of description which in some way quantifies the flexibility of each structural form within the inhomogeneous ensemble would be more appropriate for defining the relationship between structural dynamics and fluorescence yield.

We next consider the structure of LBVE. We find that LBVE is formed when water is added to acetonitrile solutions of BVE, which is nearly insoluble in water due to its strong intramolecular H-bonds in its ground state. Thus, we propose that breaking of an intramolecular H-bond and deprotonation of BVE are the two key steps for LBVE generation. In the photoexcited state, BVE can lose a proton through excited state proton transfer to the protic solvent, but a majority of the population regenerates the original species through back proton transfer in the ground state. However, a small fraction of BVE molecules lose a proton irreversibly and form LBVE which has 37-fold higher fluorescence QY than that of BVE.

Model for excited-state dynamics of BVE

In 1983, Braslavsky et al. proposed a complex scheme incorporating four configurations of BVE with interconversion paths



Scheme 1 Proposed excited-state relaxation mechanism for BVE in aprotic (left) and protic (right) solvents

involving proton transfer between the B/C rings, rotation around the C9-C10 bond in the electronic ground state, and $E \rightleftharpoons Z$ isomerization of the C10=C11 bond in the excited state.1 Their theory was mainly based on the four-component time-resolved fluorescence spectrum of BVE in solution, suggesting multiple ground state conformations. They proposed intramolecular proton transfer between the B and C pyrrole rings based on observations in closely related dipyrrole molecules, but their deuterium isotope labeling suggested that it is a minor non-radiative decay pathway. They also observed a temperature dependence of the 70 ps lifetime component in EtOH, which they assigned to C9-C10 single bond torsion.

In the current study, we did not observe timescales beyond tens of ps in aprotic solvents. A 70 ps component was not observed; however, temperature-dependent measurements were not available. We also performed viscosity-dependent measurements to more closely examine the proposed bond torsion and our results indicate that the 30 ps component is directly associated with bond torsion. Given these differences in experimental methodology, it seems reasonable to conclude that the studies are in qualitative agreement. However, the site of bond torsion cannot be determined only from the spectroscopy data and we prefer to assign it to the torsion of C15=C16 bond according to recent spectroscopy and calculation studies. 12-15

We propose a new model for the excited-state dynamics of BVE (Scheme 1). In this model, BVE in an aprotic solvent only has intramolecular H-bonding and 95% of the excited-state population returns to the ground state through a non-radiative internal conversion pathway. A picosecond excited state relaxation process is needed to achieve a luminous state (~ 30 ps) which is associated with ring twisting process. These decay processes exist in all solvents, although they might differ slightly in proportion and lifetimes. For BVE in a protic solvent, the intramolecular H-bonds are disturbed due to the unexpected H-bonding interactions with solvents and the proportion of the excited-state population returning to the ground state through the 1.9 ps internal conversion pathway decreases. All these changes result in a more efficient 0.8 ps emissive decay channel. On the other hand, after the ~ 30 ps ringtwisting process, the remaining excited-state population could reach a luminous state with a lifetime of more than 400 ps, accompanied by excited state proton transfer to the solvent. Back proton transfer could occur in the ground state, leading to most of the deprotonated BVE returning to its original state.

However, a small proportion could lose a proton irreversibly to generate LBVE.

Conclusions

Steady-state and transient spectroscopy were used to analyze the excited-state dynamics of BVE in solution from the hundreds of femtoseconds to nanosecond timescales. The key factors in the excited state dynamics are changes of the intramolecular H-bonding environment in BVE, which is disrupted by a protic solvent but stays intact in an aprotic solution, and the propensity of the D ring to lose a proton in the excited state. In protic solvents, these dynamics also lead to the emergence of LBVE, a de-protonated BVE structure with D-ring extension and a fluorescence QY much higher than that of BVE. This excited-state behavior facilitated by ring twisting and proton transfer is manifested to different degrees in solutions and most fluorescent proteins with linear tetrapyrrole chromophores, and it often plays a key role in producing functional FPs such as 'light switching'. Our results provide new insights for understanding excited-state dynamics of BVE in solvents and for exploring its properties in bilin-containing FPs.

Conflicts of interest

There are no conflicts to declare.

Acknowledgements

This study was funded by the National Natural Science Foundation of China (No. 91850202, 11674101 and 21873030 to J. C.) and the National Science Foundation Physics Frontier Center at JILA (NSF PHY 1734006 to R. J.). This work was also supported by the 111 Project (B12024). R. J. is a member of the Quantum Physics Division of the National Institute of Standards and Technology.

References

- 1 S. E. Braslavsky, A. R. Holzwarth and K. Schaffner, Angew. Chem., Int. Ed. Engl., 1983, 22, 656-674.
- 2 G. S. Filonov, K. D. Piatkevich, L.-M. Ting, J. Zhang, K. Kim and V. V. Verkhusha, Nat. Biotechnol., 2011, 29, 757.

- 3 A. Miyawaki, Nat. Methods, 2016, 13, 729-730.
- 4 E. A. Rodriguez, G. N. Tran, L. A. Gross, J. L. Crisp, X. Shu, J. Y. Lin and R. Y. Tsien, *Nat. Methods*, 2016, 13, 763-769.
- 5 E. S. Burgie, J. Zhang and R. D. Vierstra, *Structure*, 2016, 24, 448–457.
- 6 J.-F. Wang, F. Ma, H.-L. Sun, J. Zhang and J.-L. Zhang, *JBIC*, *J. Biol. Inorg. Chem.*, 2017, 22, 727–737.
- 7 N. Lenngren, P. Edlund, H. Takala, B. Stucki-Buchli, J. Rumfeldt, I. Peshev, H. Hakkanen, S. Westenhoff and J. A. Ihalainen, *Phys. Chem. Chem. Phys.*, 2018, 20, 18216–18225.
- 8 K. C. Toh, E. A. Stojkovic, I. H. M. van Stokkum, K. Moffat and J. T. M. Kennis, *Proc. Natl. Acad. Sci. U. S. A.*, 2010, **107**, 9170–9175.
- 9 F. Velazquez Escobar, P. Piwowarski, J. Salewski, N. Michael, M. Fernandez Lopez, A. Rupp, B. M. Qureshi, P. Scheerer, F. Bartl, N. Frankenberg-Dinkel, F. Siebert, M. Andrea Mroginski and P. Hildebrandt, *Nat. Chem.*, 2015, 7, 423.
- 10 S. E. Braslavsky, A. R. Holzwarth, E. Langer, H. Lehner, J. I. Matthews and K. Schaffner, *Isr. J. Chem.*, 1980, 20, 196–202.
- 11 A. D. Holzwarth, J. Wendler, K. Schaffner, V. Sundström, A. Sandström and T. Gillbro, Isr. J. Chem., 1983, 23, 223–231.
- 12 R. E. Holt, D. L. Farrens, P. S. Song and T. M. Cotton, *J. Am. Chem. Soc.*, 1989, **111**, 9156–9162.
- 13 K. Smit, J. Matysik, P. Hildebrandt and F. Mark, *J. Phys. Chem. A*, 1993, **97**, 11887–11900.
- 14 J. Matysik, P. Hildebrandt, K. Smit, A. Korkin, F. Mark, W. Gärtner, S. Braslavsky, K. Schaffner and B. Schrader, J. Mol. Struct., 1995, 348, 225–228.
- 15 A. Strambi and B. Durbeej, *Photochem. Photobiol. Sci.*, 2011, **10**, 569–579.
- 16 R. Franski and T. Kozik, J. Mass Spectrom., 2016, 52, 65-68.
- 17 M. Jia, Z. Zhou, M. Lv and J. Chen, *Chin. Chem. Lett.*, 2018, **29**, 1486–1488.
- 18 M. H. Jia, H. Yi, M. F. Chang, X. D. Cao, L. Li, Z. N. Zhou, H. F. Pan, Y. Chen, S. J. Zhang and J. H. Xu, *J. Photochem. Photobiol.*, B, 2015, 149, 243–248.
- 19 J. H. Xu, D. Toptygin, K. J. Graver, R. A. Albertini, R. S. Savtchenko, N. D. Meadow, S. Roseman, P. R. Callis, L. Brand and J. R. Knutson, J. Am. Chem. Soc., 2006, 128, 1214–1221.
- 20 Z. Chen, Y. Liu, X. He and J. Chen, *Chin. J. Chem. Phys.*, 2020, 33, 69–74.
- 21 Q. Chae and P.-S. Song, J. Am. Chem. Soc., 1975, 97, 4176-4179.
- 22 P.-S. Song, Q. Chae and J. D. Gardner, *Biochim. Biophys. Acta, Protein Struct.*, 1979, **576**, 479–495.
- 23 U. Neugebauer, A. März, T. Henkel, M. Schmitt and J. Popp, *Anal. Bioanal. Chem.*, 2012, **404**, 2819–2829.
- 24 Principles of Fluorescence Spectroscopy, ed. J. R. Lakowicz, Springer, US, Boston, MA, 2006, vol. 6, pp. 205–235.
- 25 S. E. Boiadjiev and D. A. Lightner, *Tetrahedron: Asymmetry*, 1999, **10**, 607–655.
- 26 M. a. E. Mora, S. E. Bari, J. Awruch and J. M. Delfino, *Bioorg. Med. Chem.*, 2003, 11, 4661–4672.
- 27 P. Novotná, F. Králík and M. Urbanová, *Biophys. Chem.*, 2015, **205**, 41–50.

- 28 S. E. Braslavsky, A. R. Holzwarth and K. Schaffner, Angew. Chem., Int. Ed. Engl., 1983, 22, 656–674.
- 29 C. Carreira-Blanco, P. Singer, R. Diller and J. Luis Pérez Lustres, Phys. Chem. Chem. Phys., 2016, 18, 7148-7155.
- 30 S. P. Velsko and G. R. Fleming, *J. Chem. Phys.*, 1982, 76, 3553–3562.
- 31 J. R. Taylor, M. C. Adams and W. Sibbett, *Appl. Phys.*, 1980, **21**, 13–17.
- 32 V. Sundström and T. Gillbro, *Chem. Phys.*, 1981, **61**, 257–269.
- 33 J. Claret, O. Ibars, K. Lang, F. R. Trull and D. A. Lightner, *Biochim. Biophys. Acta, Gen. Subj.*, 1995, **1243**, 221–229.
- 34 F. Celis, M. M. Campos-Vallette, J. S. Gómez-Jeria, R. E. Clavijo, G. P. Jara and C. Garrido, Spectrosc. Lett., 2016, 49, 336–342.
- 35 F. Thümmler and W. Rüdiger, *Tetrahedron*, 1983, **39**, 1943–1951.
- 36 H. P. Upadhyaya, J. Phys. Chem. A, 2018, 122, 9084-9092.
- 37 X. Cao, C. Zhang, Z. Gao, Y. Liu, Y. Zhao, Y. Yang, J. Chen, R. Jimenez and J. Xu, *Phys. Chem. Chem. Phys.*, 2019, 21, 2365–2371.
- 38 S. E. Braslavsky, A. R. Holzwarth, H. Lehner and K. Schaffner, *Helv. Chim. Acta*, 1978, **61**, 2219–2222.
- 39 E. J. Land, Photochem. Photobiol., 1979, 29, 483-487.
- 40 X. Wang, Z. Zhou, Y. Tang, J. Chen, D. Zhong and X. Jianhua, *J. Phys. Chem. B*, 2018, **122**, 7027–7037.
- 41 I. V. Polyakov, B. L. Grigorenko, E. M. Epifanovsky, A. I. Krylov and A. V. Nemukhin, *J. Chem. Theory Comput.*, 2010, **6**, 2377–2387.
- 42 G. Cui, Z. Lan and W. Thiel, J. Am. Chem. Soc., 2012, 134, 1662–1672.
- 43 D. A. Horke and J. R. R. Verlet, *Phys. Chem. Chem. Phys.*, 2012, **14**, 8511–8515.
- 44 G.-J. Huang, C.-W. Cheng, H.-Y. Hsu, C. Prabhakar, Y.-P. Lee, E. W.-G. Diau and J.-S. Yang, *J. Phys. Chem. B*, 2013, 117, 2695–2704.
- 45 B. Zietz and F. Blomgren, *Chem. Phys. Lett.*, 2006, **420**, 556-561.
- 46 M. Barbatti, J. Pittner, M. Pederzoli, U. Werner, R. Mitrić, V. Bonačić-Koutecký and H. Lischka, *Chem. Phys.*, 2010, 375, 26–34.
- 47 P. Slavicek and M. Farnik, Phys. Chem. Chem. Phys., 2011, 13, 12123-12137.
- 48 C. García-Iriepa, H. A. Ernst, Y. Liang, A.-N. Unterreiner, L. M. Frutos and D. Sampedro, *J. Org. Chem.*, 2016, 81, 6292–6302.
- 49 T. Förster and G. Hoffmann, Z. Phys. Chem., 1971, 75, 63-76.
- 50 M. K. Kuimova, G. Yahioglu, J. A. Levitt and K. Suhling, *J. Am. Chem. Soc.*, 2008, **130**, 6672–6673.
- 51 V. Modi, S. Donnini, G. Groenhof and D. Morozov, *J. Phys. Chem. B*, 2019, **123**, 2325–2334.
- 52 D. M. Leitner and P. G. Wolynes, *Chem. Phys. Lett.*, 1997, **280**, 411-418.
- 53 L. Canty, S. Hariharan, Q. Liu, S. A. Haney and D. W. Andrews, *PLoS One*, 2018, **13**, e0208075.